Virtual design and analysis of Pareto optimal emitter structures for thermophotovoltaic applications

Nari Jeon,[†] Jonathan J. Hernandez,[‡] Alex B. F. Martinson,[†] Stephen K. Gray,[¶] and Jonathan J. Foley IV[*,§]

[†]*Materials Science Division, Argonne National Labratory, Argonne, Illinois, 60439, USA*

[‡]*Union County College, 1033 Springfield Avenue, Cranford, New Jersey, 07016, USA*

[¶]*Center for Nanoscale Materials, Argonne National Labratory, Argonne, Illinois, 60439, USA*

[§]*Department of Chemistry, William Paterson University, 300 Pompton Road, Wayne, New Jersey, 07470, USA*

E-mail: foleyj10@wpunj.edu

Abstract

The ability to shape the absorption and emission profile of nanostructures by exploiting various resonant phenomena that arise in nanoscale structures has garnered significant interest in designing nanostructured selective emitters for thermal energy conversion applications such as thermophotovoltaics. In this work, we focus on composite planar structures that leverage the interaplay between two resonant phenomena that can be realized in simple planar nanostructures: resonant absorption in weakly-absorbing thin films and reflection resonances in multi-layer dielectric stacks (Bragg Reflectors). The interplay between these resonances enables spectral tunability of the

composite nanostructures, and yields structures whose thermal emission properties approach the ideal limit of a step-function emitter. We combined rigourous electrodynamics calculations with a virtual screening technique based on Pareto optimality to identify a small number of promising structures from a search space of more than 5 million structures. We identify structures that have a predicted spectral efficiency of (replace with the real number!) 65% and a predicted spectral density of (replace with the real number!) $80000 W/m^2$.

Introduction

Solar energy conversion has been explored through direct solar to electrical energy conversion via the photovoltaic (PV) effect, and solar to thermal energy, which can be efficiently stored for later use and can be converted to electric power. The conversion efficiency of solar cells based on the PV effect are limited by the broadness of the solar spectrum: photons below a PV bandgap energy cannot create current at all while photons with energy above the bandgap suffer losses through various energy disspation mechanisms. In thermophotovoltaic (TPV) systems, incoming energy is used to heat an emitting surface to high temperatures, which results in a large amount of thermal emission from the surface. This thermal emission is then captured by a low-bandgap PV cell where it is turned into electrical energy. Traditional TPV systems use waste heat or a burning fuel to heat the emitter while solar thermophotovoltaic (STPV) systems use concentrated solar energy. One of the key ideas driving the development of STPV technology is that the thermal emission of the emitter structure can be shaped in such a way that it deviates significantly from blackbody emission. In particular, one seeks to minimize thermal emission of sub-bandgap photons and maximize thermal emission in a small bandwidth at and above the bandgap energy.

If a perfect quantum efficiency for the photovoltaic is assumed, the photovoltaic power generated per unit area of the PV cell (the power density) is given simply by the flux of photons incident upon the PV with energies at or above the bandgap multipled by the

bandgap energy,

$$\rho = E_{bg} \cdot \dot{N}_{\lambda \leq \lambda_{bg}}. \tag{1}$$

This photon flux depends on the temperature and spectral properties of the emitter,

$$\dot{N}_{\lambda \leq \lambda_{bg}} = \int_0^{\lambda_{bg}} \frac{\lambda}{hc} B(\lambda, T)\, \epsilon(\lambda)\, d\lambda, \tag{2}$$

where $B(\lambda, T)$ is Planck's blackbody law as a function of wavelength and temperature, $\epsilon(\lambda)$ is the emissivity spectrum of the emitter, h is Planck's constant, and c is the vacuum speed of light. The photovoltaic power generated per unit area of the PV cell is therefore computed by

$$\rho = \int_0^{\lambda_{bg}} \frac{\lambda}{\lambda_{bg}} B(\lambda, T)\, \epsilon(\lambda)\, d\lambda. \tag{3}$$

Similarly, the efficiency of power generated from the emitter/PV pair is given by the ratio of the power generated per unit area of the PV cell divided by the optical power incident per unit area of the PV cell,

$$\eta = \frac{\rho}{\rho_{incident}}, \tag{4}$$

where $\rho_{incident}$ can again be determined from the emissivity spectrum of the emitter and Planck's blackbody distribution. Hence, the efficiency can be computed as

$$\eta = \frac{\int_0^{\lambda_{bg}} \frac{\lambda}{\lambda_{bg}} B(\lambda, T)\, \epsilon(\lambda)\, d\lambda}{\int_0^{\infty} B(\lambda, T)\, \epsilon(\lambda)\, d\lambda}. \tag{5}$$

We emphasize that the power density and efficiency quantities defined above do not take into account the quantum efficiency of the PV cell (η_{PV}) or the efficiency with with the emitter structure can be heated (η_Q); the overall device efficiency will be a produce of these three efficiencies. Because the power density and efficiency quantities depend on the spectral properties of the emitter structure, we will refer to η as the Spectral Efficiency and ρ as the Spectral Power Density throughout this work, and these will be the key figures of merit that

will be used to evaluate candidate emitter structures.

It can be seen from the above analysis that the emissivity spectrum of the emitter ($\epsilon(\lambda)$) is a key quantity in determining η and ρ for a given candidate emitter structure. For example, if $\epsilon(\lambda)$ has the form of a delta function at $\lambda = \lambda_{bg}$, then the emitter has perfect spectral efficiency ($\eta = 1$) but has negligible spectral density. Alternatively, if the emissivity spectrum has the form of a step function ($\epsilon(\lambda) = 1$ when $\lambda \leq \lambda_{bg}$ and $\epsilon(\lambda) = 0$ otherwise), then the Spectral Power Density is maximized, though the Spectral Efficiency will be less than unity. Ideal STPV systems therefore allow the entire solar spectrum to be utilized, resulting in a theoretical maximum efficiency of 85.4% based on the Carnot cycle limit [2]. The spectral shaping capabilities of nanostructured materials has created considerable interest in designing optical nanostructures to both harvest the solar spectrum through broad-band absorption and convert optical energy through spectrally selective emission. The design and integration of spectrally engineered absorber and emitter structures is a key challenge facing the realization of high-performance STPV devices. In both types of structures, conflicting performance charecteristics must be considered for pairing the solarthermal absorber/emitter device with a PV material of a bandgap wavelength (λ_{bg}). An ideal absorber will 100% of the spectral power from sub-bandgap photons and should not re-radiate any spectral power from photons at or above the bandgap energy. Practically speaking, absorption should be high for wavelengths longer than λ_{bg} and low for wavelengths shorter than λ_{bg} for high-performance STPV absorbers, which leads naturally to a bi-objective optimization problem. Emitter structures also face conflicting performance criteria. Emitter structures should maximize the radiation of spectral power from photons that precisely match the bandgap energy of a PV cell to maxize the ratio of power radiated to electrical power produced. This consideration can be formulated mathematically in terms of a figure of merit known as the spectral efficiency (SE),

$$SE = \frac{\int_0^{\lambda_{bg}} \frac{E_{bg}}{E_\lambda} \varepsilon(\lambda) B(\lambda, T) d\lambda}{\int_0^{\infty} \epsilon(\lambda) B(\lambda) d\lambda}, \tag{6}$$

where $\varepsilon(\lambda)$ is the emissivity (taken to be equal to the absorption), E_{bg} is the band-gap energy

of the PV material the absorber/emitter is paired with, and $B(\lambda, T)$ is Planck's blackbody spectrum. The form of this figure of merit leads to the conclusion that the ideal form of the emissivity is a delta function about λ_{bg}, $\delta(\lambda - \lambda_{bg})$. While such a structure will achieve the maximum possible spectral efficiency of 1, such a structure will necessarily have very low useful power density, necessitating very large emitter surface areas to enable large electrical power generation. In this context, we define useful power density (UPD) as power density resulting from photons which are capable of creating photocurrent, that is, photons with $\lambda \leq \lambda_{bg}$. Similarly, we can formulate the UPD mathematically,

$$UPD = \int_0^{\lambda_{bg}} \frac{E_{bg}}{E_\lambda} \varepsilon(\lambda) B(\lambda, T) d\lambda. \tag{7}$$

It can be seen that the two figures of merit form conflicting objectives; as the USD may be increased at the expense of the SE and vice versa. While a delta-function emissivity maximizes spectral efficiency, it can be seen that a step-function emission profile is one that maximizes useful power density. Realistic structures will have thermal emission profiles that interpolate between these two limits, and a question arises as to the optimal charecteristics of such realistic structures. Previous emitter design has focused largely on achieving spectrally selective characteristics that tend to maximize SE. For example, patterned surfaces, including a VO2-based photonic crystal with an optimal spectral efficiency (see Eq. (1)) of 54% for InGaSb PV cells with a band gap of 0.62 eV [7], W-based graded index structure with an optimal efficiency of 59% for GaSb PV cells with a band gap of 0.73 eV [5], and W-based photonic crystals with an optimal efficiency of 63% for GaSb PV cells with a band gap of 0.73 eV [8]. (Do we know the USD of any of these structures???)

Considerably less attention has been placed on designing emitter structures which maximize USD, though recent work by Wang and co-workers suggested that a step-function emissivity is ideal for STPV applications, suggesting that USD is in fact a critical figure of merit. Although the precise relationship between overall conversion efficiency of a STPV

device and the USD and SE is complex and requires many considerations about the implementation of the device itself, it is clear that both figures of merit play an important role in device performance. Given this, we wish to systematically analyze the balance of SE and USD in realistic and idealized structures. In this work, we address this question by analyzing the performance of a suite of more than 5 million structures with respect to both SE and USD for use with two common low-bandgap PV materials, GaSb ($\lambda_{bg} = 1707nm, E_{bg} \approx 0.73$ eV) and InGaAsSb ($\lambda_{bg} = 2254nm, E_{bg} = 0.55$ eV). We consider a class of 1D hybrid nanostructures that consist of an optically thick tungsten substrate, a Bragg reflector, and a weakly absorbing thin-film metal/dielectric alloy. Such structures offer several advantages: their spectral properties can be widely tuned by modifying the resonant properties of the Bragg reflector and the alloy layer, and their optical response can be computed analytically using the Transfer Matrix Method, enabling the type of extensive search space employed here. Practically speaking, this class of structure may be readily fabricated using known techniques, and the components can be made from materials that have the requisite thermal and mechanical properties to withstand high temperatures without suffering device failure. Drawing on the language of multi-objective optimization, we identify from our extensive search space the subset of Pareto optimal structures for each PV material. In our application, a Pareto optimal structure is one where modifying any of the structural parameters under consideration cannot simultaneously improve both the USD and the SE. Our analysis leads us to structures with SE of $REALLYHIGH$ with USD above $PRETTYHIGHT$, and SE of $PRETTYHIGH$ with USD above $REALLYHIGH$. (Some statement in comparison to previous structures). Furthermore, we find that our Pareto optimal structures display M^{th} (fill in with real number) order scaling in USD and N^{th} order scaling in SE with Temperature. By comparison, a step function emitter shows M^{th} (fill in with real number) order scaling in USD and N^{th} order scaling in SE with Temperature and a delta function emitter shows linear scaling in USD and constant SE as a function of Temperature. (some conclusion about this).

Theory

Transfer Matrix Method

All of our structures can be classified as L-layer planar structures with variations only along the $z-$axis and that are isotropic along the $x-$ and $y-$axes. This structure greatly simplifies the theoretical treatment of the optical response, as the fields can be written in a piece-wise fashion as plane waves, and closed-form expressions for the wavevectors and amplitudes of the fields in each layer can be determined from considerations of Maxwell's equations and appropriate boundary conditions. The boundary conditions can be expressed conveniently as matrix equations, and the amplitudes can be computed by straightforward matrix multiplication, which forms the basis of what is called the Transfer Matrix Method.[?]

The general Transfer Matrix equations for an L-layer system can be written as

$$\begin{pmatrix} E_1^+ \\ E_1^- \end{pmatrix} = \begin{pmatrix} M_{1,1} & M_{1,2} \\ M_{2,1} & M_{2,2} \end{pmatrix} \begin{pmatrix} E_L^+ \\ E_L^- \end{pmatrix}, \tag{8}$$

where the elements $M_{i,j}$ depend on the material properties (the refractive index, n) and geometry of each layer, as well as the frequency and polarization of incident light. This formalism assumes that layer 1 and layer L are semi-infinite materials with real refractive indices; however, all intermediate layers have finite thickness and may consist of materials with complex refractive indices. The 2x2 $\mathbf{M}$ matrix above can be computed from the following matrix product,

$$\begin{pmatrix} M_{1,1} & M_{1,2} \\ M_{2,1} & M_{2,2} \end{pmatrix} = \mathbf{D}_1^{-1} \left(\prod_{l=2}^{L-1} \mathbf{D}_l \, \mathbf{P}_l \, \mathbf{D}_l^{-1} \right) \mathbf{D}_L. \tag{9}$$

The $\mathbf{P}$ matrix is defined for each finite-thickness layer as

$$\mathbf{P}_l = \begin{pmatrix} \exp(i\,\phi_l) & 0 \\ 0 & \exp(-i\,\phi_l) \end{pmatrix}, \tag{10}$$

where $\phi_l = k_{z,l}\, d_l$ where d_l is the thickness of the l^{th} layer of the structure,

$$k_{z,l} = \sqrt{\left(n_l\,\frac{\omega}{c}\right)^2 - \left(n_1\,\sin(\theta_1)\,\frac{\omega}{c}\right)^2} \tag{11}$$

θ_1 is angle of incidence of light of frequency ω upon the structure, and n_l is the refractive index of the l^{th} layer. If the incident light is s-polarized, then the $\mathbf{D}$ matrix for layer l has the form

$$\mathbf{D}_l = \begin{pmatrix} 1 & 1 \\ n_l\cos(\theta_l) & -n_l\cos(\theta_l) \end{pmatrix}, \tag{12}$$

while the $\mathbf{D}$ matrix has the form

$$\mathbf{D}_l = \begin{pmatrix} \cos(\theta_l) & \cos(\theta_l) \\ n_l & -n_l \end{pmatrix}, \tag{13}$$

if the incident light is p-polarized. Again, n_l is the refractive index of the l^{th} layer, and θ_l is the angle of refraction in the l^{th} layer, which is governed by Snell's law.[?]

The amplitudes E_1^+ and E_1^- are interpreted as incoming and outgoing wave amplitudes on the incident side, respectively; similarly, E_L^- and E_L^+ are incoming and outgoing wave amplitudes, respectively, on the terminal side of the structure. With the access to the field amplitudes and wavevectors, a number of useful quantities may be computed. For example, the Fresnel reflection and transmission amplitudes may be computed as $r = E_1^-/E_1^+$. The reflection can then be calculated as $R = |r|^2$, the transmission as $T = |t|^2\; n_L cos(\theta_L)/(n_1 cos(\theta_1))$, where n_i and θ_i denote the refractive index of the material of layer i and the incident/refraction angle in layer i, respectively. The absorption at a given

frequency, which we take to be equal to the emissivity by Kirchoff's law, can simply be computed as $\varepsilon(\omega) \equiv A(\omega) = 1 - T(\omega) - R(\omega)$, where $\varepsilon(\omega)$ is the emissivity. The computational effort of the Transfer Matrix Method is minimal and arises mainly from the effort required to compute the matrix elements $M_{i,j}$. From Eq. 9, it can be seen that the effort required to evaluate the **M** matrix grows linearly with the number of layers in the structures. This feature of the TMM makes our large-scale computational screening approach feasible even with modest computational resources.

Critical Coupling

Our structures draw inspiration from a coupled photonic crystal/weak absorber system recently described by Piper and Fan. In their particular work, a single layer of graphene (the weak absorber) is shown to exhibit perfect resonant absorption when placed atop a 2D siliocon photonic crystal under conditions known as critical coupling. Analogously, we take a thin-film of tungsten-alumina alloy to be our weak absorber layer, and we couple this absorbing layer to a Bragg Reflector. Both components can be viewed as resonators, and both components can have their resonant properties tuned through simple parameters. For the tungsten-alumina alloy, the absorption resonance position and linewidth can be varied via the volume fraction of tungsten. For the Bragg Reflector, the reflection resonance position and linewidth can be modified by the opitcal thickness and dielectric contrast of the alternating layers. Under the condition that the absorption resonance and the reflection resonance have the same frequency, the absorption of the coupled system may be derived from coupled mode theory[?]

$$A(\omega) = \frac{4\gamma_A \, \gamma_{BR}}{(\omega - \omega_0)^2 + (\gamma_A + \gamma_{BR})^2}, \tag{14}$$

where γ_{BR} is the leakage rate of the Bragg Reflector and γ_A is the intrinsic loss rate of the absorbing layer. The γ_A term may be determined from the half-width at half-max (HWHM) of the resonant absorption line, which may be computed via a TMM calculation on the

absorbing layer bounded from above and below by vacuum (or an appropriate dielectric medium). Similarly, γ_{BR} may be determined by considering the HWHM of the stored-energy spectrum of the BR, where the stored-energy $|E_{BR}|^2$ at a given frequency may be computed from the TMM as

$$|E_{BR}|^2 = \frac{1}{2\gamma_{BR}}(r+1)(r^*+1) \equiv \frac{1}{2\gamma_{BR}}\left(\frac{M_{2,1}}{M_{1,1}}+1\right)\left(\left(\frac{M_{2,1}}{M_{1,1}}\right)^*+1\right). \tag{15}$$

Alloys Effective Medium Theory

We model the alloy layer using an effective medium theory, which maintains the isotropy of this layer in the $x-$ and $y-$ planes. In this work, the alloy is considered to consist of uniformly distributed spherical inclusions of tungsten metal embedded in alminum oxide. Such an alloy can be readily fabricated using a technique like atomic layer deposition. We apply Maxwell Garnett theory to compute the effective dielectric function of our alloy,

$$\epsilon_{alloy} = \epsilon_D \frac{2v_F\left(\epsilon_W(\omega)-\epsilon_D\right)+\epsilon_W(\omega)+2\epsilon_D}{2\epsilon_D+\epsilon_W(\omega)+v_F\left(\epsilon_D-\epsilon_W(\omega)\right)}, \tag{16}$$

where $\omega_W(\omega)$ is the dielectric function of Tungsten, ϵ_D is the dielectric function of alumina, and v_F is the volume fraction of the tungsten inclusions. From the above discussion, it can be seen that our search space includes the following structural parameters: volume fraction of the alloy layer (v_F), the number of periods in the Bragg Reflector (Λ), as well as the thickness of the layers in the Bragg Reflector (d_1 and d_2). We fix the thickness of the alloy layer to be 20 nm, and we fix the composition of the Bragg Reflector layers to be SiO_2 (n=1.45) and Ta_2O_5 (n=2.10). The emissivity can therefore be seen to be a function of these four variables, in addition to frequency: $\varepsilon(\omega, v_F, d_1, d_2, \Lambda)$. From the defintion of the SE and USD, it can be seen that temperature and λ_{BG} are also important parameters. Consequently, we can see that the spectral efficiency and useful spectral density are functions of the structural parameters, the band gap, and the temperature: $SE(v_F, d_1, d_2, \Lambda, T, \lambda_{BG})$

and $USD(v_F, d_1, d_2, \Lambda, T, \lambda_{BG})$.

The search space of each parameter save λ_{BG} is discretized into 20 equally spaced values. We search values of the volume fraction between v_F min and v_F max, values of d_1 between $d_1 minand d_1 max$, values of d_2 between $d_2 minand d_2 max$, values of Λ between $NLminandNLmax$, and values of T between $1000 and 1700K$. We consider two values of λ_{BG}: 1707 nm corresponding to GaSb cells, and 2254 nm corresponding to InGaAsSb cells.

Pareto Front

We apply a virtual screening approach based on identifying the set of Pareto optimal solultions with respect to the SE and USD, where a Pareto optimal solution is one that is not *dominated* by any other solutions in the search space. For the particular bi-optjective search considered in this work, a solution $\mathbf{x_i}$ is dominated by the solution $\mathbf{x_j}$ if $SE(\mathbf{x_j}) \geq SE(\mathbf{x_i})$ and $USD(\mathbf{x_j}) \geq USD(\mathbf{x_i})$ and either $SE(\mathbf{x_j}) > SE(\mathbf{x_i})$ or $USD(\mathbf{x_j}) > USD(\mathbf{x_i})$. Put another way, no solutions exist in the search space that simulateneously have higher SE and USD values than the Pareto optimal solutions. The set of Pareto optimal solutions is referred to as the Pareto front.

Results

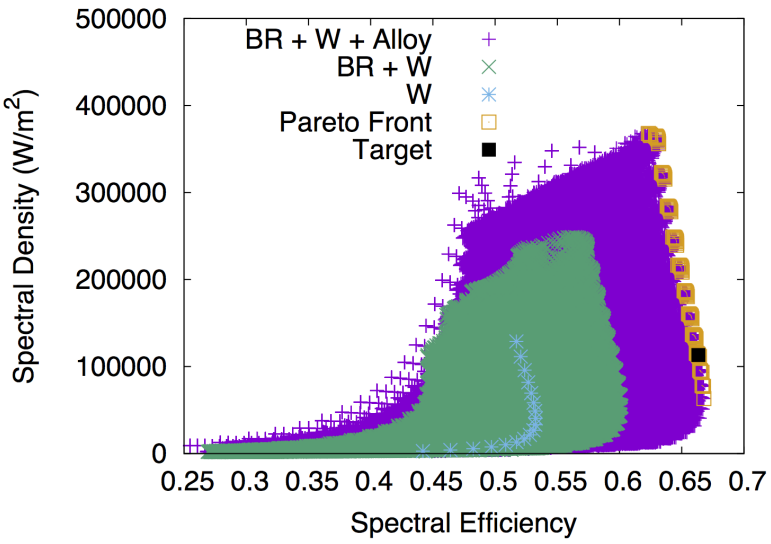

Figure 1: Comparison of possible values for Spectral Density and Spectral Efficency for a variety of planar structures at temperatures between 1200K and 2200K when $\lambda_{bg} = 2254$nm. The class of planar structures include optically-thick tungsten (denoted 'W'), variable Bragg reflectors with an optically-thick tungsten substrate (denoted 'BR + W'), and variable W/Alumina alloys with variable Bragg reflectors with an optically-thick tungsten substrate (denoted 'BR + W + Alloy'). It is seen that in each case, the additional degrees of freedom added by the additional structures enhances optimal Spectral Efficiencies and Spectral Densities, hence the Pareto front for the entire solution space corresponds to 'BR + W + Alloy' structures. One such Pareto optimal structured is targetted for fabrication (denoted 'Target'). The dielectric function of the alloy in this search is computed using Maxwell-Garnett theory utilizing bulk dielectric function values for W[?] and experimentally-derived dielectric function values are used for the ALD alumina.

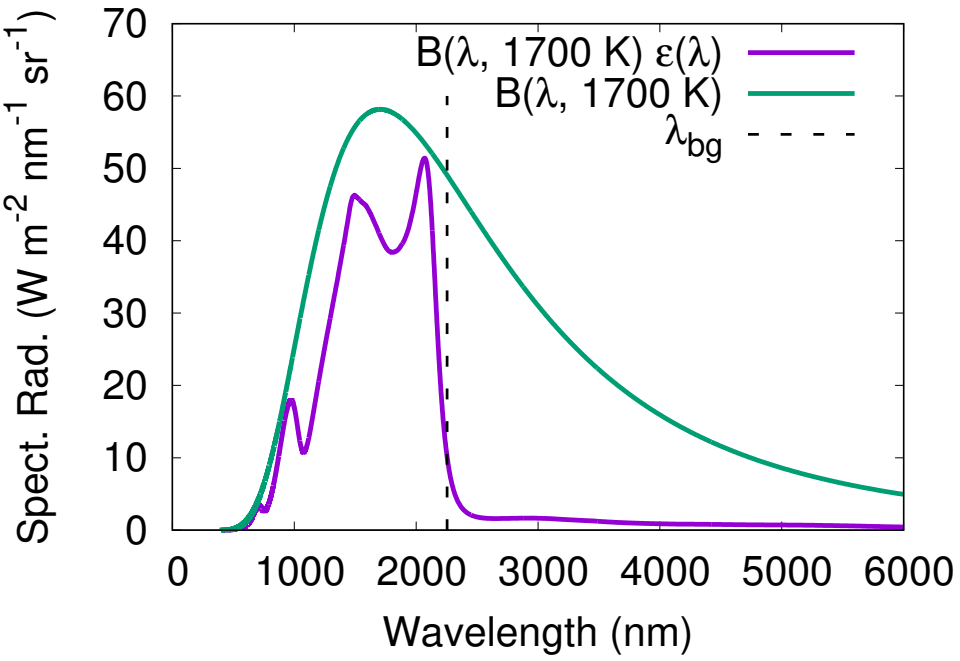

Figure 2: **(a)** Theoretical normal thermal emission spectrum of Target structure compared to Blackbody emission at 1700 K. Under Lambertian approximation, spectral efficiency is 66% and spectral density is 1.05e+5 W/m^2. The geometry of the target structure is depicted in panel **(b)**.

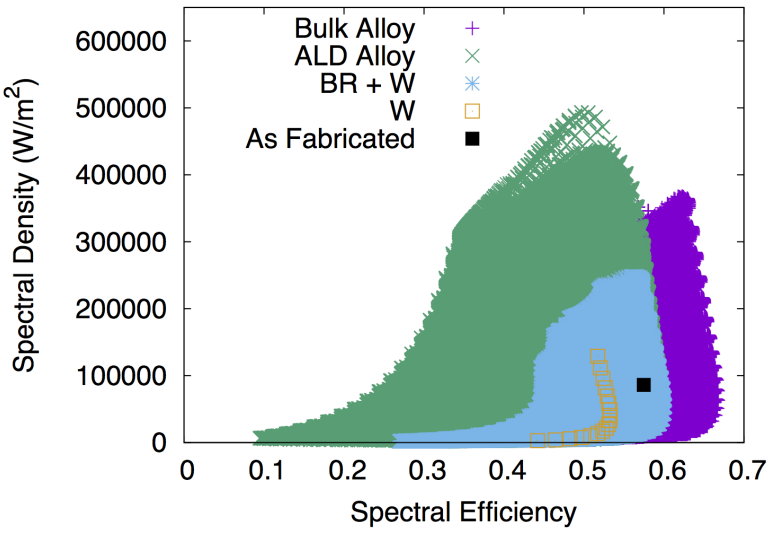

Figure 3: Comparison of possible values for Spectral Density and Spectral Efficency for a variety of planar structures and different alloy models at temperatures between 1200K and 2200K when $\lambda_{bg} = 2254$nm. Two alloy models are considered: one that utilizes Maxwell-Garnett theory and bulk dielectric function values for tungster? (labeled 'Bulk Alloy'), and one that utilizes Bruggenman theory and dielectric function values from ellipsometry performed on ALD tungsten (labeled 'ALD Alloy). The ALD Alloy model is found to provide better agreement with fabricated structures. It is seen that the additional degrees of freedom afforded by the ALD Alloy increases the spectral density, but not the spectral efficiency, relative to the tungsten substrate/Bragg reflector structure. The As-Fabricated structure that is experimentally characterized lies close to the Pareto front of the ALD Alloy structures.

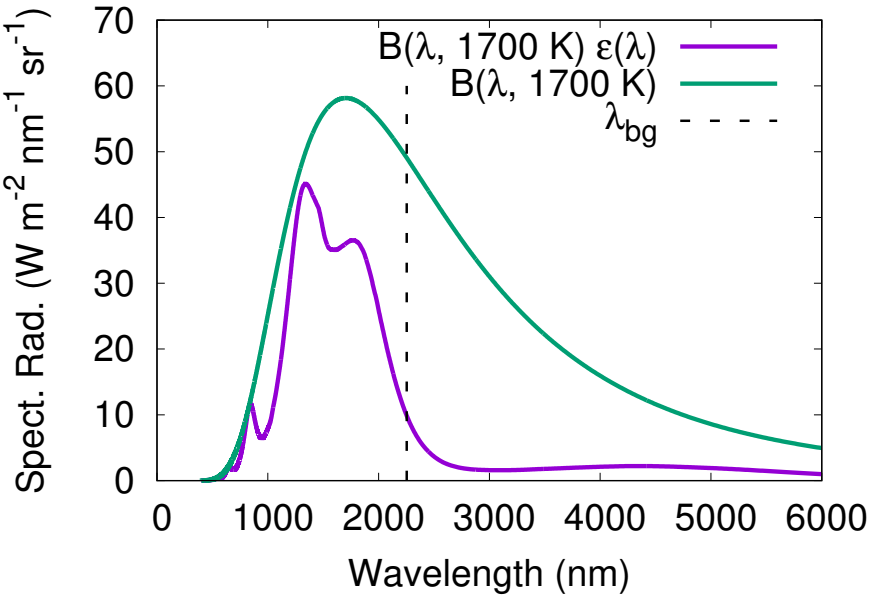

Figure 4: **(a)** Theoretical normal thermal emission spectrum of Target structure compared to Blackbody emission at 1700 K. Under Lambertian approximation, spectral efficiency is 57% and spectral density is 8.60e+5 W/m^2. The geometry of the target structure is depicted in panel **(b)**.

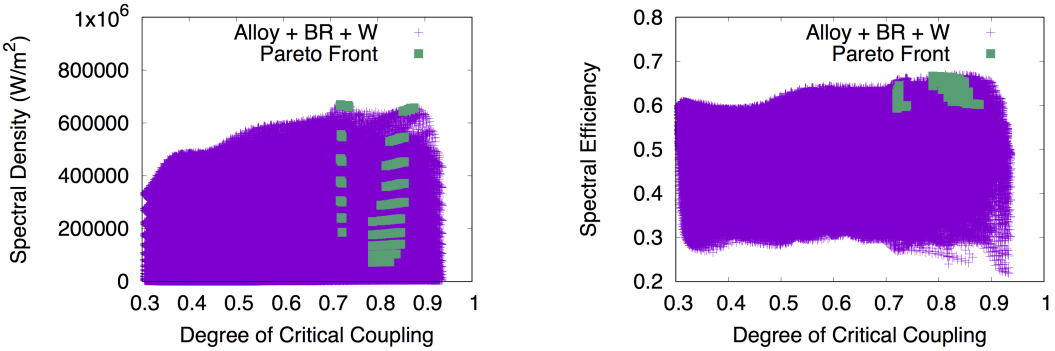

Figure 5